Erschienen in: Nanotechnology ; 19 (2008), 46. - 465603

A simple low temperature synthesis route for ZnO–MgO core–shell nanowires

N O V Plank[1,5], H J Snaith[2], C Ducati[3], J S Bendall[1], L Schmidt-Mende[4] and M E Welland[1]

[1] Nanoscience Centre, Department of Engineering, The University of Cambridge, 11 J J Thomson Avenue, Cambridge CB3 0FF, UK
[2] Clarendon Laboratory, Department of Physics, University of Oxford, Parks Road, Oxford OX1 3PU, UK
[3] Department of Materials Science, Pembroke Street, Cambridge CB2 3QZ, UK
[4] Ludwig-Maximilians University (LMU) Munich, Department of Physics and Center for NanoScience (CeNS), Amalienstrasse 54, 80799 Munich, Germany

Abstract

We report a hydrothermal synthesis method for MgO shell coatings directly onto the surface of ZnO nanowire arrays. The entire process can be carried out below 100 °C. The MgO shells are produced by the addition of 10 mM magnesium nitrate with 0.2 M sodium hydroxide in water, resulting in a shell thickness of up to 8 nm, verified by high resolution transmission electron microscopy. The viability of the MgO layer as a functional element of optoelectronic devices was tested on solid-state organic hole-transporter based dye-sensitized solar cells. Incorporation of the MgO shell into the solar cell resulted in substantive efficiency improvements of over 400% in comparison to the pristine ZnO nanowire based photovoltaics, indicating that electrons can efficiently tunnel through the 'insulating' MgO shell.

(Some figures in this article are in colour only in the electronic version)

1. Introduction

In the field of nanotechnology, the synthesis of controlled structures is crucial for the development of functional devices, with many in the field aiming for the convenience of bottom up fabrication as opposed to timely and costly top down methods. Progress therefore depends on reliable routes to low cost and scalable nanostructures with useful functional properties [1]. Low temperature synthesis of nanostructures, such as quantum dots [2, 3], and nanowires [4, 5], are a key area of importance, with device applications in various fields [1–3, 5]. ZnO is a wide bandgap (3.2 eV) semiconducting material, usually n-type due to defects and non-stoichiometry, with good chemical stability [6, 7], making it useful in solar cells [8, 9], light emitting diodes [10, 11], gas sensing devices [12, 13] and transistors [14]. Recently, there have been many reports of ZnO nanowire (NW) devices [6, 7, 15], with interest stemming from the facile synthesis of aligned and uniform ZnO NW arrays by low temperature (below 100 °C) hydrothermal methods [16, 17]. In addition to hydrothermal synthesis, there is a wealth of information on the synthesis of ZnO NWs using chemical vapour deposition for high quality transistor devices, which require high temperature processing, ranging from 400 to 1050 °C [5–7, 14, 18].

Due to the higher defect density introduced by the low temperature chemical route employed in the growth of ZnO NWs, it may be advantageous to passivate the surface of the NWs to control the surface reactivity and limit the electronic influence of surface defects [7]. A common technique to control and enhance the properties of nanostructures is to create core–shell heterostructures [2, 3, 6, 15, 19, 20]. The addition of a shell often modifies the electronic nature of the original material, by enhancing the interaction with the surrounding medium without altering the properties, both optical and electrical, of the core structure. Some specific examples of MgO as a shell to a metal oxide semiconducting core were developed using high temperature synthesis routes. Previously, researchers have fabricated

[5] Author to whom any correspondence should be addressed.

controlled ZnO–MgO (nanopillar) heterostructures [5, 6, 15], which may be useful in the study of chemical sensors, optical devices and scanning probes in addition to providing a reliable heterojunction material to study quantum confinement effects. High temperature sintering of colloidal aqueous solutions has been developed as a method for producing SnO_2/MgO core–shell nanocrystals for liquid electrolyte dye-sensitized solar cells [21]. Similarly, doping ZnO with MgO in an aqueous solution to produce a flat film, followed by a high temperature anneal, has also been observed to be particularly useful in hybrid solar cell devices as a form of bandgap engineering [22]. Bandgap engineering is a technique employed in conventional solid-state semiconductor solar cells to increase device efficiencies by tuning the donor density in the semiconductor [23]. Core–shell NWs of ZnO/TiO_2 have also been fabricated using a high temperature ∼350 °C atomic layer deposition method, and they were found to enhance dye-sensitized solar cell performance.

Here we report a low temperature, solution-based controllable growth route to fabricate MgO shells directly onto ZnO NW surfaces. To the best of our knowledge this is the first reported method which does not require a subsequent high temperature annealing stage, with the entire synthesis being possible under 100 °C, thereby making the synthesis compatible with flexible substrate requirements and reel-to-reel processing. To test the performance of the ZnO–MgO core–shell NWs in hybrid photovoltaic devices, solid-state dye-sensitized solar cells (SDSCs) were constructed, incorporating the molecular hole-transporter 2,2′,7,7′-tetrakis(*N*,*N*-di-*p*-methoxyphenylamine)-9,9′-spirobifluorene (spiro-OMeTAD). This is also the first demonstration of ZnO NWs incorporated into this class of solar cell. We observe the overall efficiency of SDSCs incorporating these NW films to increase from 0.07% for a pristine NW device to 0.33% in the ZnO–MgO core–shell devices, an almost five-fold improvement, which demonstrates the utility of a buffer layer in this system.

2. Experimental details

2.1. Nanowire core–shell synthesis

Core–shell nanowire structures were grown by hydrothermal growth methods [16], in a two-stage process. (1) Deposition of the Zn seed layer followed by the hydrothermal growth of ZnO NWs. (2) Deposition of the MgO shell onto the ZnO core by low temperature hydrothermal growth. For all devices indium tin oxide (ITO) on glass substrates were cleaned in acetone and IPA following standard substrate cleaning procedures in a cleanroom environment. A 250 nm (approximately) layer of Zn metal was sputtered directly onto the clean ITO substrate, which acts effectively as the seed layer. It should be noted that, in contrast to other reports where the ZnO seed layer is also fabricated using a high T anneal stage (>300 °C) [9, 24, 25], the sputter deposition process for the zinc layer used here is compatible with many substrate materials, including flexible substrates, in addition to being advantageous for solar cell device characteristics [26].

For the NW synthesis, the growth solution for hydrothermal preparation of ZnO was prepared by mixing 0.025 M zinc nitrate hydrate and 0.025 M hexamethylenetetramine (HMT) in water. The nanowire growth was then carried out by placing the Zn coated ITO on glass substrates directly into the growth solution. The solution was held at 92 °C for 120 min, before removing the substrates and cleaning them in deionized (DI) water. Subsequently, the films were dried on a hot plate at 100 °C to remove any excess water.

The ZnO–MgO core–shell NW structures were then fabricated by a second hydrothermal growth procedure. ZnO NW arrays were submerged in a 10 mM solution of magnesium nitrate mixed with 0.2 M NaOH at either 98.5 °C for 40 min using a water bath for even temperature (ZnO–MgO-98) or in an autoclave sealed in an oven at 120 °C for 40 min (ZnO–MgO-120). The 120 °C temperature is still compatible with flexible substrate processing requirements.

2.2. Solid-state dye-sensitized solar cell fabrication

To fabricate the SDSCs both the MgO coated and the pristine ZnO NW samples were submerged in an acetonitrile:tert-butanol (1:1) solution of a ruthenium bypyridyl NCS complex (0.5 mM) for 4 h in the dark, after which the samples were rinsed in anhydrous acetonitrile (ACN). The hole transporting material used in the SDSC was spiro-OMeTAD (Merck), which was dissolved in chlorobenzene (CB) (180 mg ml^{-1}). Tertbutyl pyridine (tbp) was added straight to the solution (1:57 tbp:CB). Lithium trifluoromethyl sulfonylimide (Li-TFSI) (ionic dopant) was separately predissolved in acetonitrile at 170 mg ml^{-1}, and then added to the hole-transporter solution at 1:27 vol:vol, as reported previously [27, 28]. To complete the devices, 50 nm thick silver top electrodes were deposited by thermal evaporation under high vacuum.

2.3. Microscopy and photovoltaic characterization

The nanowire array morphology was confirmed by scanning electron microscopy (SEM) using a LEO 1530 VP microscope. Transmission electron microscopy (TEM) analysis was performed on a FEI Tecnai F20, with 200 kV acceleration voltage, to assess the structure of the MgO shell grown hydrothermally. The spectral response of the solar cells was characterized using a tungsten lamp in combination with a monochromator and Si-reference diode, and the current–voltage response was measured with a Keithley 237 SMU under simulated sun light generated from a 300 W Oriel solar simulator calibrated using a Si-reference cell bought and calibrated from the Fraunhofer Institute of Solar Energy, with the solar cell mismatch factor accounted for.

3. Results and discussion

3.1. ZnO–MgO core–shell nanowire synthesis

A typical example of a nanowire array is shown in figure 1, showing the long range uniformity and relatively high density of our nanowire films. The NWs are approximately 500 nm long and 20–50 nm in diameter. The spacing between NWs

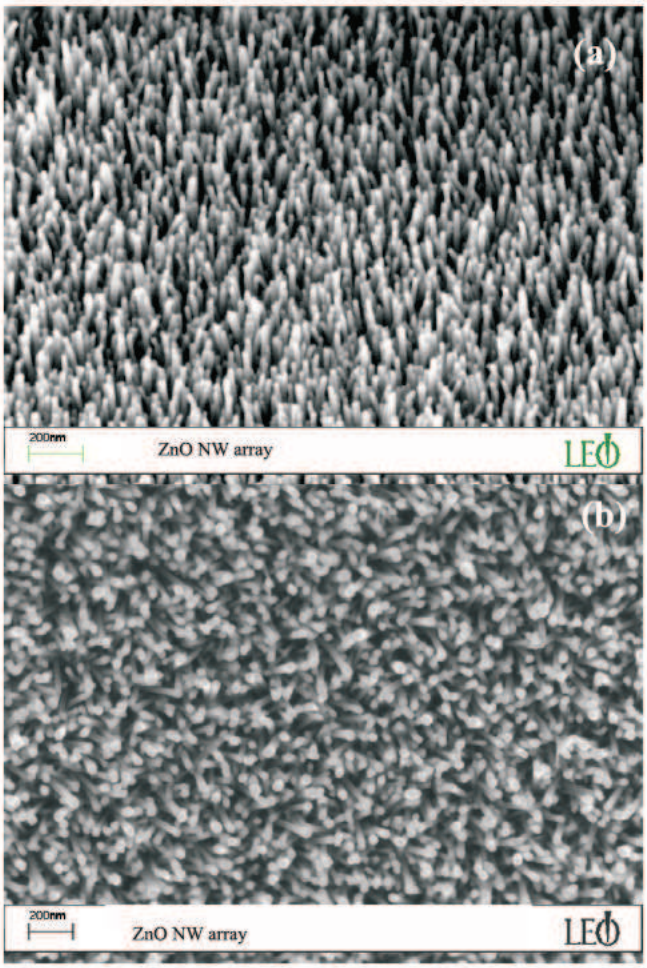

Figure 1. SEM images of the pristine ZnO NW arrays: (a) a tilted view, (b) from the top.

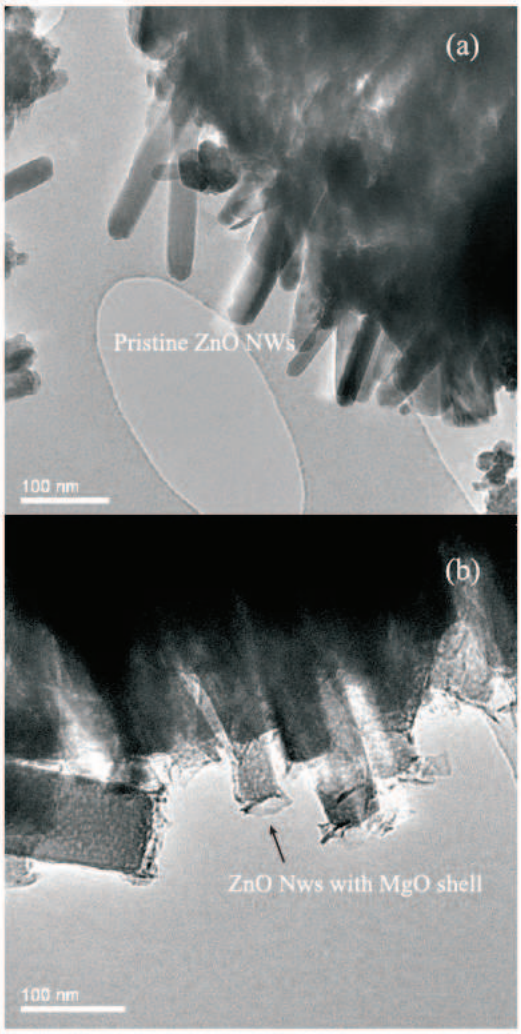

Figure 2. Bright field TEM images of (a) pristine ZnO NWs, and (b) ZnO–MgO-98 NW core–shell sample.

is slightly irregular: figure 1(b) shows a top view, where the tendency for the NWs to tilt towards each other is seen. The NWs are not perfectly aligned, with the densely packed NWs contributing 85–90% of the volume. It is known that the synthesis method employed here is advantageous for selective area patterning as the densely packed NW arrays will only form in the areas patterned with the Zn seed region, which could be controlled lithographically.

The bright field, medium magnification images of figure 2 show a comparison between (a) pristine ZnO NWs, and (b) ZnO–MgO-98 core–shell NWs (MgO-98 refers to the 98.5 °C synthesis route for the MgO coating). The morphology and diameter distribution of the ZnO nanowires look similar in both images, but in figure 2(b) the thin MgO shells are clearly visible, and they appear to be tight and uniform along the body of the nanowires, while flaring around the wire tip. Figure 3 shows high resolution TEM images of (a) a pristine ZnO NW, (c) a ZnO–MgO-98 core–shell NW, and (e) a ZnO–MgO-120 core–shell NW. By TEM, the NWs are observed to be single-crystal wurtzite-type ZnO. In figures 3(c) and (e) a reasonably conformal coating over the entirety of the ZnO surface is observed, with a thickness of approximately 6–8 nm, for the Mg nitrate precursor growth. Through fast Fourier transform (FFT) analysis of the high resolution TEM images, it is also possible to confirm that the growth axis of the ZnO nanowires corresponds to the *c* axis of the wurtzite unit cell, i.e. the [0001] direction, as is commonly reported [16, 17]. An example of this analysis is shown in figure 3(b). The MgO shell, which was also identified by energy-dispersive x-ray (EDX) analysis, appears to be amorphous. A typical EDX spectrum of the core–shell structure is reported in figure 3(f).

The growth process carried out here was demonstrated at two temperatures, 98.5 and 120 °C, as described in section 2. The growth of ZnO using zinc nitrate and HMT hydrothermal methods is known to take place at temperatures ranging from 40 to 95 °C [29], the temperature required for the zinc nitrate to decompose. However, common practice is to carry out the growth at approximately 90 °C, where high quality single-crystalline ZnO NWs are observed. Here, we have compared a similar hydrothermal process for the MgO shells, where the magnesium nitrate will decompose at 95 °C. Similarly to the ZnO NW literature, we have employed a growth process at an elevated temperature of 120 °C to be sure of complete decomposition and to look for improvements in the fabrication

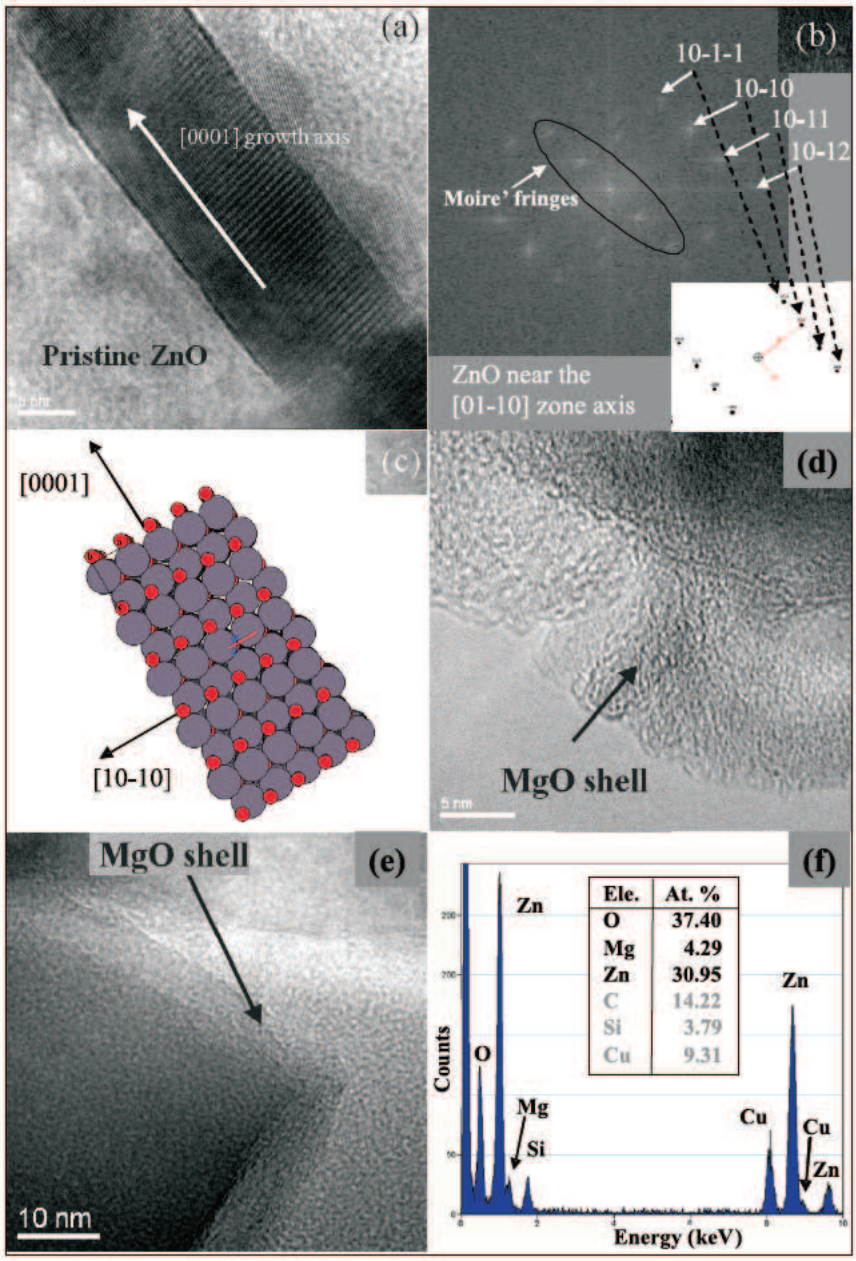

Figure 3. High resolution TEM images of (a) a single-crystal wurtzite-type ZnO NW with lattice fringes corresponding to the $(10\bar{1}0)$ planes, (d) the amorphous MgO shell of a ZnO–MgO-98 NW, and (e) the ZnO–MgO-120 NW core–shell sample seen at lower magnification. In (b) the FFT analysis of the NW in (a) is reported, together with (c) a ball-and-stick computer model to illustrate how the growth axis of the wire corresponds to the [0001] direction of the crystal. (f) shows the EDX spectrum taken from an isolated ZnO–MgO nanowire. The inset table contains the quantification for the elements in the core–shell structure (Cu, C, and Si are due to the substrate and TEM grid). The atomic content of Zn, Mg, and O supports the hypothesis of stoichiometric ZnO and MgO formation.

process. As both temperatures produce similar ZnO–MgO core–shell NWs, figure 3, we have verified the success of the sub-100 °C fabrication process. This low temperature synthesis method appears to be a highly effective means for studying the influence of MgO layers on ZnO structures and offers a low temperature scalable fabrication procedure. Although it could be of concern that the MgO shell is not crystalline it should be noted that other fabrication techniques for ZnO–MgO heterostructures, such as metal organic vapour phase epitaxy (MOVPE) growth, can produce amorphous MgO shells even at temperatures of above 400 °C [5].

The synthesis route employed here holds further advantages. As is the case for the ZnO NW hydrothermal synthesis, the aspect ratio and length of the NWs can be controlled by changing the concentrations of the precursors and the length of time of the reactions [17], believed to be as follows:

$$(CH_2)_6N_4 + 6H_2O \rightarrow 6HCHO + 4NH_3 \quad (1)$$

$$NH_3 + H_2O \leftrightarrow NH_4^+ + OH^- \quad (2)$$

$$2OH^- + Zn^{2+} \rightarrow ZnO(s) + H_2O. \quad (3)$$

The use of a hydrothermal synthesis of MgO directly onto the surface of predefined ZnO NWs also allows structural control and is inherently capable of producing a shell on any ZnO structure formed either hydrothermally or by any high temperature synthesis method. We propose here that the reactions in the MgO shell synthesis are as follows; the growth is shown schematically in figure 4:

$$Mg(NO_3)_2 + 2NaOH \rightarrow Mg(OH)_2(s) + 2NaNO_3 \quad (4)$$

$$Mg^{2+}(aq) + 2OH^-(aq) \rightarrow Mg(OH)_2(s) \quad (5)$$

$$Mg(OH)_2 \rightarrow MgO + H_2O. \quad (6)$$

For the concentrations used here of 10 mM solution of magnesium nitrate mixed with 0.2 M NaOH, assuming complete dissociation of the reactants, the solution will be strongly alkaline, with a pH of 13.3. The use of magnesium nitrate for these shells was inspired by the use of $Mg(NO_3)_2$ to create synthetic hydrotalcites [30], where a basic solution was required to form structures. Indeed NaOH was required in this synthesis method, as without it, no conformal MgO coatings were observed. Other work in which the coating of ZnO NWs has been extensively investigated has shown that the pH of the solution was critical to the surface characteristics of ZnO [31]. When ZnO is in contact with water the surface becomes hydrolysed, the ZnOH layer will be soluble in water, especially at the elevated pH of >13 here [31]. The Mg^{2+} in aqueous solution then has a favourable reaction site on the surface of the NWs, resulting in the core–shell structures being fabricated. The exact character of the ZnO–MgO interface is still under study, although the TEM analysis performed thus far has shown a distinct region of crystalline ZnO in the core and amorphous MgO on the shell. However, it is also possible that, due to the hydroscopic nature of MgO, the outer surface actually becomes magnesium hydroxide, as shown in equation (4). Indeed we hypothesize that the precipitation of $Mg(OH)_2$ is the driving force in the synthesis reaction. The brief anneal of the substrates at 100 °C post rinse and prior to the dye deposition (as described in section 2) could be satisfactory for the removal of excess water and reducing the Mg hydroxide to MgO. A high temperature anneal above 400 °C would unambiguously result in MgO, with the removal of all surface OH; however, such a process would be incompatible with flexible substrate requirements and would significantly increase the cost of this fabrication procedure. For a 40 min growth time the shell thicknesses ranged between 6 and 15 nm over ten samples, with an average of 8 nm; the growth has been repeated many times and the samples viewed by TEM to ensure the accuracy of the procedure and the level of control required to make reproducible nanostructures. In the CVD synthesis methods producing ZnO–MgO core–shell structures, the MgO is epitaxially grown from the ZnO surface [5], and in the growth procedure here, the native OH groups on the ZnO NW surface would act as a site for MgO growth. As yet, it is unknown whether there is a clear break at the interface, or an area of a composite material, which would subsequently alter the bandgap of the material, as has been seen in the formation of $ZnO_{(1-x)}MgO_x$ films [22] used in hybrid solar cells. The low temperature synthesis method here, with controlled alteration of the bandgap, would satisfy one of the main criteria of a nanofunctional system and could be comparable to the high temperature methods for ZnO–MgO nanopillars [5, 15] and other functional core–shell nanostructures [2–4, 19].

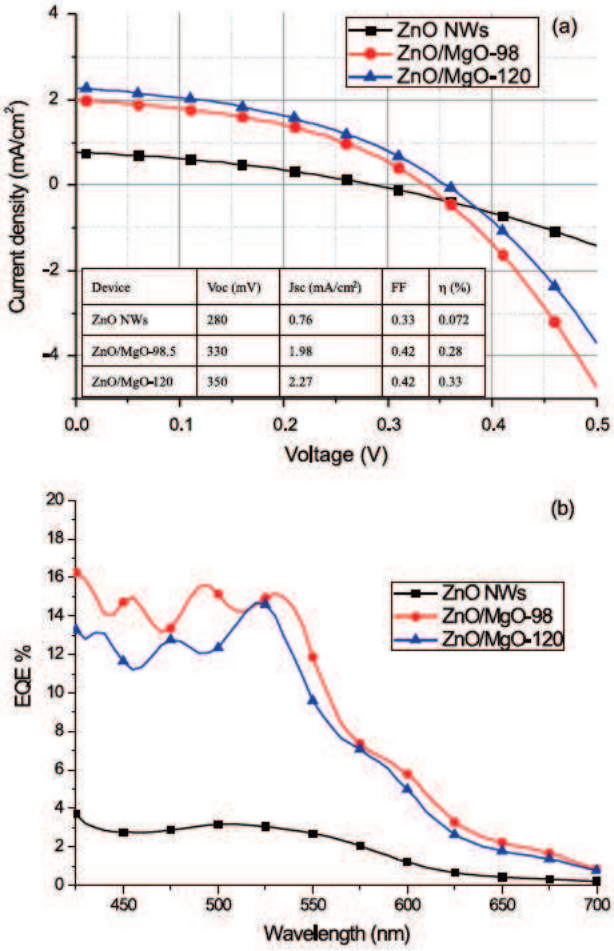

Device	Voc (mV)	Jsc (mA/cm²)	FF	η (%)
ZnO NWs	280	0.76	0.33	0.072
ZnO/MgO-98.5	330	1.98	0.42	0.28
ZnO/MgO-120	350	2.27	0.42	0.33

Figure 4. (a) The I–V characteristics of the dye/spiro-OMeTAD devices prepared from pristine ZnO NW films are compared to those prepared from ZnO–MgO-98, and ZnO–MgO-120 NW films. The table inset summarizes the solar cell performance for each of the devices. In (b) the external quantum efficiency (EQE) of the same devices is shown: the MgO coated NW films have a structured response in the 425–575 nm spectral range.

3.2. Solar cells incorporating ZnO–MgO core–shell NWs exhibiting enhanced performance

The functionality of these ZnO–MgO core–shell nanowires has been tested by fabricating solid-state dye-sensitized solar cells. The current–voltage characteristics and the photovoltaic action spectra for solid-state dye-sensitized solar cells incorporating ZnO nanowires with and without MgO coatings are shown in figures 4(a) and (b), respectively. The open-circuit voltage (V_{oc}), short-circuit current (J_{sc}), fill factor (FF) and device efficiency (η) are all listed in table 1 in the inset for each device. The first remarkable point to notice is that even though we deposit a 6–8 nm thick 'insulating' MgO shell between the semiconductor and the dye, we observe a significant

enhancement of the photocurrent with the MgO/ZnO devices: the J_{sc} measured under full sun conditions has increased from 0.8 to 2.3 mA cm^{-2}. The addition of an MgO layer has led to an increase in the open-circuit voltage of approximately 70 mV, from 280 mV in the pristine sample, up to 350 mV in the device incorporating the core–shell nanowires. Figure 5(b) shows the clear difference between the photovoltaic action spectra of the pristine sample in comparison to the ZnO–MgO-98 and ZnO–MgO-120 core–shell NW devices. The external quantum efficiencies (EQEs) at 550 nm in these devices are observed to be around 3%, 14% and 12% respectively. In general the deviations between ZnO–MgO-98 and ZnO–MgO-120 are negligible.

The three-fold increase in the J_{sc} of the ZnO–MgO core–shell NW devices appears to follow from the enhanced adsorption of more dye on the MgO layer, in comparison to the pristine ZnO sample. Since these films are so thin and have a relatively low dye loading, resolving the dye absorption using transmission spectrophotometry is challenging. However, in figure 5, it is apparent that the samples with the MgO shells do scatter light more strongly, which will be advantageous for increasing the optical path-length and ensuing light capture in the films. The spectral response curves appear to have features beyond that of the dye absorption; see figure 4(b). Since these films are weakly absorbing and the top Ag electrode will be acting as a mirror, a standing wave will be set up with a node in the optical power density at the mirror. Clearly the positioning of this standing wave will vary with the wavelength of the light, essentially stretching with increasing wavelength, and hence the integrated optical power density in the film will also vary resulting in further structure to the spectral response. Optical modelling of the system is beyond the scope of this work.

Further to optical scattering effects, the MgO shell is likely to play a role enhancing the solar cell performance through several mechanisms. The first issue to consider is the adsorption of dye on the MgO surface. In a liquid electrolyte dye-sensitized solar cell study [21], the addition of a MgO shell to SnO_2 core nanoparticles greatly improved the adsorption of the dye, as probed by UV–vis spectroscopy, leading to an enhancement of device efficiency by approximately six times. Similarly, the dye adsorption onto pristine ZnO structures is known to be problematic, with a tendency for dye molecules to agglomerate [32]. The EQE for ZnO DSSCs has been shown to reach a maximum after only 2 min exposure time [32], whereas here the samples were submerged in the dye for 4 h. Consequently the pristine ZnO NW samples may have sub-optimal dye loading, whereby dye agglomeration could limit the charge transfer. The ZnO surface is known to be unstable in acidic environments and it is therefore likely that the dye is detrimentally harming the ZnO surface. In contrast, the amorphous MgO coating may improve the dye adsorption, inhibiting the agglomeration effects and hence allowing good charge transfer characteristics, as indicated by figure 4(b). The MgO will also have enhanced stability in the acidic dye solution. Also, as well as improving the dye adsorption, the MgO coating appears to increase the scattering of light by the film and hence light absorption; see figure 5. An increase in surface roughness from the MgO coating is to be expected

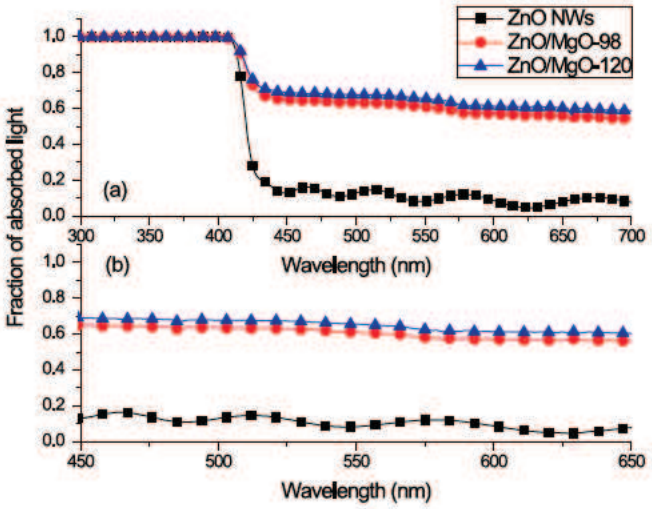

Figure 5. (a) UV–visible fraction of absorbed light spectra for pristine ZnO, ZnO–MgO-98, and ZnO–MgO-120 NW films, with dye for 4 h adsorption, and coated with spiro-OMeTAD as detailed in the device fabrication procedure. The plot in (b) is an enlarged version of (a) showing the increase in light absorbance induced by the 8 nm MgO shell coating.

in comparison to the smooth crystalline surface of the ZnO NWs, therefore leading to an increase in surface area for dye molecules to attach in addition to an increase in light scattering, resulting in an enhanced photocurrent.

It is also necessary to consider the electronic structure of the sub-10 nm hydrothermal MgO shell. Several methods exist in the literature for the improvement of excitonic solar cell device performance [33, 34], which involve coating n-type mesoscopic electrode structures in 'passivating' layers. An atomic layer deposition (ALD) method to apply 10 nm of TiO_2 directly onto ZnO NWs [35] in hybrid solar cells has been employed to improve the device performance to a power conversion efficiency from 0.04% to 0.29%. In organic polymer photovoltaic devices, a layer by layer step system at the 10 nm scale has been employed to create a controlled physical separation between layers of the solar cell; the efficiency increased to 0.26% [36] from an initial 0.025% with a single junction by reducing the likelihood of back recombination, whilst still allowing charge transfer. Similarly, molecular interface modification in a hybrid bilayer device has shown an efficiency increase from 0.34% to 0.6%. In the more mature field of liquid electrolyte dye-sensitized solar cells, the use of metal oxides as a coating layer for the mesoscopic n-type material has shown device improvements [37], as has increasing the insulating chain length of the photoactive dye molecules in SDSCs [38]. The latter case indicates that the dye itself can inhibit, or at least influence, the recombination between electrons in the TiO_2 with holes in the spiro-MeOTAD. The use of a metal oxide insulating layer is the closest example to the devices made here; an 8 nm insulating layer of aluminium oxide improved the solar cell efficiency [37]. It is reasonable to suppose that the physical separation induced by the insulating shell or coating between the hole and electron may reduce the chances of charge recombination and therefore enhance the solar cell

performance. It must also be noted that the improvement of these ZnO–MgO core–shell devices could be due to altering of the bandgap, similarly to the addition of MgO into ZnO films [22] or in CVD ZnO–MgO nanopillars [5, 15], allowing for interstitial states to create injection paths enhancing the J_{sc}, as an intermediate band solar cell [39]. It is evident that the MgO coatings we have fabricated promote effective electron tunnelling through mid-gap states, and the detailed mechanism is under further investigation.

4. Conclusion

The novel low temperature hydrothermal synthesis of ZnO–MgO core–shell NWs described above is a successful and inexpensive method of producing uniform, functional nanostructures. The hydrothermal synthesis can produce MgO coating of controlled thickness and it can be applied to any ZnO structure. This method can be adopted to coat a variety of metal oxide materials. The hydrothermally grown MgO layers enhance the photocurrent and open-circuit voltage of solid-state dye-sensitized solar cells, producing a five-fold increase in power conversion efficiency, as measured under AM1.5 simulated sun light. Further optimization, investigation of the charge generation mechanism and increase in nanowire length and surface area are being actively pursued, which should lead to considerable performance enhancements and a competitive hybrid photovoltaic system.

Acknowledgments

The authors would like to thank the Optoelectronics Group in the Cavendish Laboratory, led by Professor Richard Friend, for discussions and equipment access. CD wishes to thank the Royal Society for funding. NOVP wishes to thank the FP6 Frontiers Network of Excellence and the IRC in Nanotechnology funded by the EPSRC. This work was also partially funded by EPSRC grant EP/F056702/1. JSB acknowledges funding from the EU FPS project, STABILIGHT. We also thank Shaik M Zakeeruddin and Michael Grätzel from EPFL for supplying the ruthenium complex sensitizer.

References

[1] Hodes G 2007 When small is different: some recent advances in concepts and applications of nanoscale phenomena *Adv. Mater.* **19** 639
[2] Alivisatos A P 1996 Semiconductor clusters, nanocrystals, and quantum dots *Science* **271** 933–7
[3] Mews A *et al* 1994 Preparation, characterization, and photophysics of the quantum dot quantum well system cadmium sulfide/mercury sulfide/cadmium sulfide *J. Phys. Chem.* **98** 934–41
[4] Rao C N R, Vivekchand S R C V, Biswas K and Govindaraj A 2007 Synthesis of inorganic nanomaterials *Dalton Trans.* **34** 3728
[5] Heo Y W *et al* 2004 ZnO nanowire growth and devices *Mater. Sci. Eng.* R **47** 1–47
[6] Klingshirn C 2007 ZnO: material, physics and applications *ChemPhysChem* **8** 782
[7] Schmidt-Mende L and MacManus-Driscoll J L 2007 ZnO-nanostructures, defects, and devices *Mater. Today* **10** 40–8
[8] Olson D C *et al* 2006 Hybrid photovoltaic devices of polymer and ZnO nanofiber composites *Thin Solid Films* **496** 26–9
[9] Law M *et al* 2005 Nanowire dye-sensitized solar cells *Nat. Mater.* **4** 455–9
[10] Ryu Y *et al* 2006 Next generation of oxide photonic devices: ZnO-based ultraviolet light emitting diodes *Appl. Phys. Lett.* **88** 241108
[11] Franky S *et al* 2007 Recent progress in solution processable organic light emitting devices *J. Appl. Phys.* **102** 091101
[12] Xu J *et al* 2000 Grain size control and gas sensing properties of ZnO gas sensor *Sensors Actuators* B **66** 277–9
[13] Wan Q *et al* 2004 Fabrication and ethanol sensing characteristics of ZnO nanowire gas sensors *Appl. Phys. Lett.* **84** 3654–6
[14] Sun B and Sirringhaus H 2005 Solution-processed zinc oxide field-effect transistors based on self-assembly of colloidal nanorods *Nano Lett.* **5** 2408–13
[15] Kling R, Th Gruber C K, Reuss F and Waag A 2004 Analysis of ZnO and ZnMgO nanopillars grown by self-organization *Nanotechnology* **15**
[16] Vayssieres L 2003 Growth of arrayed nanorods and nanowires of ZnO from aqueous solutions *Adv. Mater.* **15** 464
[17] Li Q *et al* 2005 Fabrication of ZnO nanorods and nanotubes in aqueous solutions *Chem. Mater.* **17** 1001–6
[18] Cha S N *et al* 2006 High performance ZnO nanowire field effect transistor using self-aligned nanogap gate electrodes *Appl. Phys. Lett.* **89** 263102–3
[19] Kim S *et al* 2008 Growth and enhanced light emission of hybrid structures of ZnO/Si nanocrystals *Appl. Phys. Lett.* **92** 243108–3
[20] Lee S S *et al* 2008 Homogeneous ZnS coating onto TiO_2 nanoparticles by a simple one pot sonochemical method *Chem. Eng. J.* **139** 194–7
[21] Boateng O-A, Asoka Kumara S K, Okuya M, Murakami K, Konno A and Tennakone K 2005 Sensitization of nanocrystalline SnO_2 films with indoline dyes *Japan. J. Appl. Phys.* **44** 731
[22] Olson D C, Shaheen S E, White M S, Mitchell W J, van Hest M F A M, Collins R T and Ginley D S 2007 Band-offset engineering for enhanced open-circuit voltage in polymer-oxide hybrid solar cells *Adv. Funct. Mater.* **17** 264
[23] Yu K M *et al* 2003 Diluted II–VI oxide semiconductors with multiple band gaps *Phys. Rev. Lett.* **91** 246403
[24] Ravirajan P *et al* 2006 Hybrid polymer/zinc oxide photovoltaic devices with vertically oriented ZnO nanorods and an amphiphilic molecular interface layer *J. Phys. Chem.* B **110** 7635–9
[25] Baxter J B and Aydil E S 2006 Dye-sensitized solar cells based on semiconductor morphologies with ZnO nanowires *Sol. Energy Mater. Solar Cells* **90** 607–22
[26] Plank N O V *et al* 2008 The backing layer dependence of open circuit voltage in ZnO/polymer composite solar cells *Thin Solid Films* **516** 7218
[27] Snaith H J *et al* 2006 Light intensity, temperature, and thickness dependence of the open-circuit voltage in solid-state dye-sensitized solar cells *Phys. Rev.* B **74** 045306
[28] Snaith H J *et al* 2006 Dye-sensitized solar cells incorporating a 'liquid' hole-transporting material *Nano Lett.* **6** 2000–3
[29] Guo M *et al* 2005 The effect of hydrothermal growth temperature on preparation and photoelectrochemical performance of ZnO nanorod array films *J. Solid State Chem.* **178** 3210–5
[30] Das J, Das D and Parida K M 2006 Preparation and characterization of Mg–Al hydrotalcite-like compounds containing cerium *J. Colloid Interface Sci.* **301** 569–74
[31] Grasset F *et al* 2003 Surface modification of zinc oxide nanoparticles by aminopropyltriethoxysilane *J. Alloys Compounds* **360** 298–311

[32] Keis K *et al* 2000 Studies of the adsorption process of Ru complexes in nanoporous ZnO electrodes *Langmuir* **16** 4688–94
[33] Gregg B A 2003 Excitonic solar cells *J. Phys. Chem.* B **107** 4688–98
[34] Gledhill S E, Scott B and Gregg B A 2005 Organic and nano-structured composite photovoltaics: an overview *J. Mater. Res.* **20** 3167–79
[35] Greene L E *et al* 2007 ZnO–TiO_2 core–shell nanorod/P3HT solar cells *J. Phys. Chem.* C **111** 18451–6
[36] Benten H, Ogawa M, Ohkita H and Ito S 2008 Design of multilayered nanostructures and donor–acceptor interfaces in solution-processed thin-film organic solar cells *Adv. Funct. Mater.* **9999** NA **18** 1563
[37] Palomares E *et al* 2003 Control of charge recombination dynamics in dye sensitized solar cells by the use of conformally deposited metal oxide blocking layers *J. Am. Chem. Soc.* **125** 475–82
[38] Schmidt-Mende L *et al* 2005 Effect of hydrocarbon chain length of amphiphilic ruthenium dyes on solid-state dye-sensitized photovoltaics *Nano Lett.* **5** 1315–20
[39] Martí A *et al* 2006 Novel semiconductor solar cell structures: the quantum dot intermediate band solar cell *Thin Solid Films* **511/512** 638–44